# Organic Xerogel and PVDF derived Carbon Nanostructures as Anode materials for Lithium Ion Batteries

M.G. Karthik

(CH13M1005)

A Dissertation Submitted to

Indian Institute of Technology Hyderabad

In Partial Fulfillment of the Requirements for

The Degree of Master of Technology

भारतीय प्रौद्योगिकी संस्थान हैदराबाद

Indian Institute of Technology Hyderabad

Department of Chemical Engineering

June, 2015

# Declaration

I declare that this written submission represents my ideas in my own words, and where others' ideas or words have been included, I have adequately cited and referenced the original sources. I also declare that I have adhered to all principles of academic honesty and integrity and have not misrepresented or fabricated or falsified any idea/data/fact/source in my submission. I understand that any violation of the above will be a cause for disciplinary action by the Institute and can also evoke penal action from the sources that have thus not been properly cited, or from whom proper permission has not been taken when needed.

_Karthik M.G_

(Signature)

(M G Karthik)

(CH13M1005)

# Approval Sheet

This thesis entitled **"Organic Xerogel and PVDF derived Carbon Nanostructures as Anode materials for Lithium Ion Batteries"** by **M. G. Karthik** is approved for the degree of Master of Technology from IIT Hyderabad.

**Dr. Saptarshi Majumdar**
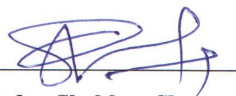IIT Hyderabad
Examiner

**Dr. Debaprasad Shee**
IIT Hyderabad
Examiner

**Dr. Ashok Kumar Pandey**
IIT Hyderabad
Examiner

**Dr. Chandra Shekhar Sharma**
IIT Hyderabad
Adviser

# Acknowledgements

Karthik M.G
30-06-2015

Dear Chandra and All,

Thanks for sending Karthik's thesis.  The thesis reads good and in line with the requirement of MTech thesis.

I do not have any specific comments regarding his thesis. From my point of view, it is approved.

Thanks and regards,

Ashok

**Dedicated to**

My Parents

# Abstract

The main aim of this present study is to understand how changes in hard carbon microstructure affects the electrochemical performance when used as anode for Lithium-Ion Batteries. We have explored two hard carbon precursors: resorcinol formaldehyde based xerogel and polyvinylidene fluoride (PVDF) polymer. Depending upon the precursors and synthesis conditions hard carbons differ in their microstructure in terms of crystallinity, porosity, morphology and also in the heteroatoms content and functional groups. To enhance the electrochemical performance we used different synthesis parameters like optimizing ball milling duration in case of resorcinol formaldehyde based carbon xerogel and pyrolysis temperature in case of PVDF. In order to understand the various structural changes we performed different characterization like Brunauer-Emmett-Teller, Transmission Electron Microscopy, Scanning Electron Microscopy, X-ray diffraction, RAMAN spectroscopy and Fourier Transform Infrared Spectroscopy. Further, we performed Galvanostatic charge/discharge experiments, Impedance spectroscopy and cyclic voltammetry to gauge the electrochemical performance.

We studied the effect on ball milling on the structure of resorcinol formaldehyde derived carbon xerogel and efforts were made to correlate its electrochemistry with the microstructural changes. We were able to improve the performance of carbon xerogel powder further by inducing more disorder in these hard carbons. The electrochemical performance was evaluated for 100 cycles at 0.1 C rate and also further tested at higher C rates. The sample ball milled for 4 hours yielded a reversible capacity of 242 mAh/g after 100 cycles. It was further tested for its rate capability up to 1 C. It recovered 85 % of the initial capacity when cycled backed at 0.1 C rate. Thus the 4 hours ball milled sample was found to be the best in terms of reversible capacity, and cyclability and rate capability. Thus by ball milling, we were not only able to enhance the reversible capacity but also improve its rate capability.

We have also studied the effect of temperature on carbon derived from PVDF. PVDF derived carbon in powder form has been tested as an anode for lithium ion battery. Its practical usage was impaired because of low yield (20 %) and high irreversible capacity. To remove the fluorine, increase the carbon content and improve the yield we first partially dehydrofluorinated the sample. The dehydrofluorination acts as a thermal stabilization step. Further we also studied the effect of atmosphere on dehydrofluorination reaction. We then pyrolyzed the dehydrofluorinated samples and studied the changes in functional groups at

different temperatures. Although we have shown that the electrochemical performance improves with improvement in crystallinity with increase in pyrolysis temperature but there is still need to either modify its microstructure by ball milling or pyrolyzing at further higher temperature for significant improvement in reversible capacity.

# Nomenclature

| | |
|---|---|
| BET | Brauner Emmett Teller |
| CDA-900 | Carbon derived from PDA at 900°C |
| CDI-1200 | Carbon derived from PDI at 1200°C |
| CDI-900 | Carbon derived from PDI at 900°C |
| FESEM | Field Emission Scanning Electron Microscope |
| HRTEM | High Resolution Transmission Electron Microscope |
| PDA | PVDF dehydrofluorinated in air |
| PDI | PVDF dehydrofluorinated in inert atmosphere |
| PVDF | Polyvinylidene fluoride |
| RFCX | Resorcinol Formaldehyde derived Carbon Xerogel |
| RFCX-15 | RFCX ball milled for 15 mins |
| RFCX-240 | RFCX ball milled for 240 mins |
| RFCX-45 | RFCX ball milled for 45 mins |
| RFCX-720 | RFCX ball milled for 720 mins |
| SEI | Solid Electrolyte Interphase |
| XRD | X-ray Diffraction |

# List of Tables

# List of Figures

# Table of Contents

# Scientific Contributions from This Work

**Manuscripts Submitted (under review):**

1. K. M. Gopalakrishna; Manohar Kakunuri; Chandra S. Sharma; "Effect of Disorder Induced By Ball Milling on the Electrochemical Performance of Catalytically Graphitized Carbon Xerogel as Anode for Lithium Ion Batteries", ECS Transactions

**International Conferences Proceedings:**

1. K. M. Gopalakrishna; Manohar Kakunuri; Chandra S. Sharma; "Effect of Disorder Induced by Ball Milling on the Electrochemical Performance of Catalytically Graphitized Carbon

Xerogel As Anode for Lithium Ion Batteries", 227th Electrochemical Society meeting, May 24-28, 2015, Chicago, USA.

# Chapter 1

# Introduction

### 1.1 Introduction to lithium ion battery

A battery is a device which is used to convert chemical energy into electrical energy. A battery consists of anode, cathode and electrolyte. There are two types of batteries primary and secondary. Primary batteries are non -rechargeable while secondary batteries are rechargeable.

Li - ion battery is the commercially used secondary battery powering laptops, mobiles and now being explored for electronic vehicles as well. The term Li-ion is used because of unique principle of intercalation of Li-ions in to the host lattice structure .The Li-ions can reversibly intercalate and de-intercalate thus enabling charging and discharging of battery. In the 1990s, Sony first introduced the lithium –ion battery into market which has then since became indispensable. The advantages of Li-ion battery when compared to other secondary batteries are light weight, small size, higher energy density, low self discharge and absence of memory effect.(1).

### 1.1.1 Working mechanism of Li-ion battery
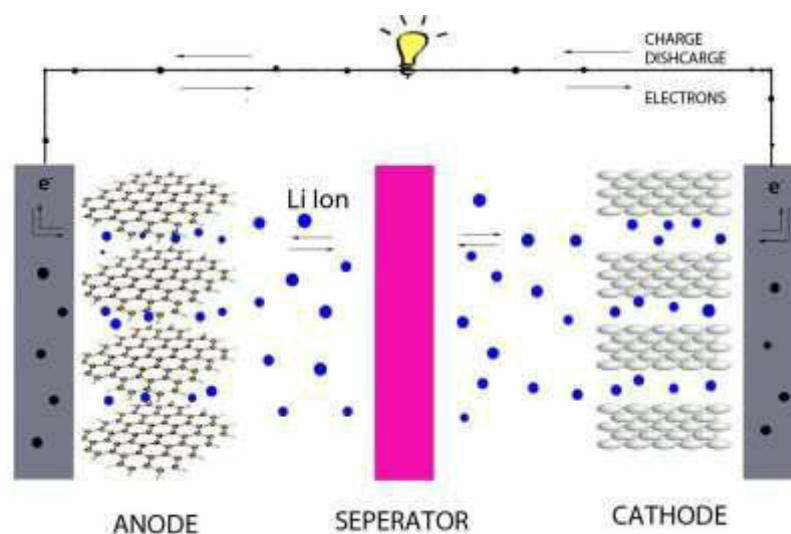


Figure 1: Schematic of a lithium ion battery.

A li-ion battery consists of two electrodes which are capable to accommodate ionic form of lithium. The two electrodes are separated by a porous membrane. A lithium salt dissolved in organic carbonate solution is used as the electrolyte. During discharging, the lithium ions are extracted from the cathode, the lithium ions diffuse through the electrolyte and gets intercalated into the carbon host structure. An equivalent amount of electrons flow through the external circuit. While charging the lithium ions from the host structure gets de-intercalated and reacts with the incoming electrons and forms lithium and gets deposited on the cathode. For intercalation six carbon atoms are required to intercalate one lithium ion.

During the first cycle, the electrolytes cannot withstand the low potential and thus reacts with lithium and carbon and forms a passivating layer called Solid Electrolyte Interphase (SEI).The SEI layer comprises of Lithium alkyl Carbonates , oxides and halides. Though there is a lot of capacity loss attributed in the first cycle due to SEI layer formation (2) The SEI layer improves the safety of the electrode by preventing it from further reacting with the electrolyte at higher negative voltage.

If the Li-ions are deposited into the host lattice structure then it is called intercalation otherwise it is called insertion. Some of the insertion mechanisms (3) are as follows:

a) Li-ion storage in the form of $Li_2$ covalent molecules.

b) Li-ion storage in cavities and pores.

c) Li-ion adsorption on both the sides of graphene sheets.


### 1.1.2 Carbon as anode materials for lithium ion battery

Sony developed the Li-ion battery first time in 1991 with Carbon as the anode. Carbon was preferred as the anode material because of its good conductivity, lower redox potential. Charge-transfer resistances at the interface between the electrolyte and active electrode materials is also small in case of carbon. Carbon is a ubiquitous element and exists in different allotropic forms like graphite, diamond and amorphous carbon and now with nanostructuring new allotropes like nanofibers, nanotubes, buckyballs and graphene have also been synthesized. The amorphous carbon can be divided into two types, hard carbon and soft carbon. Hard carbons are difficult to graphitize while soft carbons can be graphitized at higher temperatures.

Graphite is $sp^2$ hybridized carbon. They have layers of aromatic rings stacked parallel in a hexagonal fashion and bound by weak van der Waal's forces. They are excellent conductors because of delocalization of electrons possible in their $sp^2$ hybridized state. Graphite is the

widely use anode material in Li-ion battery. Though it is theoretically limited to 372mAh/g it is still used because it is easily available and inexpensive. Intercalation of one lithium requires six carbon atoms and primarily Li-ion storage is possible only due to intercalation mechanism. The advantage of graphite is its flat discharge voltage profile due to which current need not compensate for loss in voltage and thus offers constant current during discharge (4).

Soft carbons have small crystallites arranged uniformly in a very short range order. At high temperatures (~ 900 ° C) they align and thus gets graphitized. Soft carbons give higher capacity because of insertion mechanisms operating in addition to intercalation mechanism. Li-ions may get inserted into nanocavities and may react with Hydrogen terminated edges. The disadvantage is that they have low density, large irreversible capacity and poor cycleability (5).

Hard carbons consists of a very random arrangement of small crystallites arranged like a house of cards (6).They possess a lot of structural disorder .They are difficult to graphitize even at higher temperatures (~ 3000 ° C). Here the high capacity is attributed to the Li-insertion in small nanopores. Though hard carbons has disadvantages like low density and capacity degradation at higher current densities (5) they are the most promising anode material because of higher capacities it is capable of delivering.

Hard Carbons are obtained by the pyrolysis of an organic precursor. Depending on the precursor and temperature program hard carbons vary in microstructure like crystallinity, morphology, amount of heteroatoms, porosity and functional groups. All the microstructural changes play an important role in electrochemistry. Crystallinity helps in improving the conductivity. The morphology like a fractal or interconnected structure helps in facile diffusion of Li-ions (7). The density of the particles in the anode depends on the porosity, if the particle is porous then it is less dense and thus the particles are less densely packed and hence the movement of Li-ions is affected (8). The presence of heteroatoms (9) and functional groups (10) also affect the capacity. Thus a careful selection of precursors and pyrolysis program helps in developing high capacity hard carbon based anodes.


## 1.2 Objectives

The main objective of the work is to understand how different synthesis condition help us to optimize the performance of hard carbons. Hard carbons performance depends on the precursor and synthesis conditions. To study the effect of microstructure we explored ball

milling as a nanostructuring tool and evaluated its cycleability and rate capability. In order to understand how surface functional groups and crystallinity affect the performance, we pyrolyzed dehydrofluorinated PVDF at different temperatures and tested its electrochemical performance.

## 1.3 Layout of the thesis

The thesis first begins with a brief introduction to lithium ion battery mechanism before focusing on different carbon materials that are used as an anode for lithium ion battery.

In chapter 2, we have ball milled resorcinol formaldehyde derived carbon xerogel for different duration and studied the microstructural changes in detail by various characterization. We have also explained the enhanced electrochemistry in terms of these microstructural changes.

In chapter 3, we used PVDF as a precursor for hard carbon and studied the changes in surface functional groups and crystallinity with temperature. We have also studied its effect on electrochemistry. Finally in chapter 4, we summarize the major findings of this work and discuss the future directions.

# Chapter 2

# Effect of Ball Milling on the Electrochemical Performance of Catalytically Graphitized Carbon Xerogel as Anode for Lithium Ion Batteries

## 2.1 Introduction

Ball milling is the process of mechanical grinding of inhomogeneous powders to obtain powders of uniform grains size, texture and morphology. The main parameters in milling are milling duration, charge ratio (ratio between balls and powders weights), size and nature of the balls, rotation speed and filling rate of the vial (ratio between ball volume and powder volume to total vial volume) (11). Ball milling has been extensively used for carbonaceous materials to study the structural changes with change in milling time (12-16). Recently there was a report on synthesis of bi-layer graphene by ball milling graphite (17). Ball milling has been used for each type of carbon materials such as graphitic and non-graphitic both. The common effect observed is decrease in crystallinity and increase in disorder as ball milling allows breakage of weaker van der Waals bonds between the graphene layers and then fractures the graphene layers from within (18).

Carbon materials after ball milling when tested and used as anode material for Li-ion battery have demonstrated an improvement in their electrochemical performance. This improvement had been attributed due to increase in disorder (18, 19) , Li-ions insertion into voids, micro cavities (20), Li-ion reacting at the edge layers of graphene sheets (20,21), Li-ions reacting with surface functional groups (21) and formation of potato (spherical) shaped particles and aggregation (22).

5

In our present work, we have focused on ball milling of resorcinol-formaldehyde derived carbon xerogel (RFCX). Resorcinol formaldehyde xerogel is an organic gel obtained by sub-critical drying of resorcinol formaldehyde sol (23). RFCX is an example of hard carbon which is being explored as anode material for Li ion battery in recent times (24, 25) due to its several merits such as easily tunable physiochemical properties, higher carbon yield. However unlike other hard carbon materials, Li ion intercalation capacity values for different forms of RFCX as reported in literature are not promising. For example, reversible capacity for RFCX powder (24) and thin film (25) is reported to be 145 and 195 mAh/g respectively which are significantly less even than that of graphitic carbon.

As stated above, one of the major objective of this work is to improve the electrochemical performance of RFCX by milling it for different times. Although hard carbon lack any long range order in their microstructure, ball milling may create further structural disorderness in these hard carbons that will increase the reversible capacity further as reported in some of the literature (18,19). However, there is no systematic study available reporting the role of microstructure in these hard carbons which play a key role in the improvement of their electrochemical performance. Further whatever studies are available, these are limited to only few cycles of galvanostatic charge/discharge (18, 19) and therefore remain impractical for real applications of these materials as anode for Li ion battery. This provides another motivation for this work. We have studied in detail the effect of ball milling on RFCX on its microstructure and made efforts to understand its role to improve the electrochemical performance not only in terms of reversible capacity but also considered cyclability and high rate capability for these materials.

## 2.2 Materials and method

*Materials*

Resorcinol (99% purity), formaldehyde (37% w/v; stabilized with about 10% methanol), potassium carbonate (98% purity), LP-30 electrolyte (1 M $LiPF_6$ in 1:1 v/v mixture of ethylene carbonate and diethyl carbonate) were procured from Merck, India. Lithium foil (99.9% trace metal basis) and Iron (II) acetate were procured from Sigma Aldrich, India. We used stainless steel (SS) foil (polycrystalline SS 316, 100 µm thick) as current collector and procured the same from MTI corp., USA. Deionized water was used as solvent for preparing resorcinol formaldehyde sol. All chemicals were used directly without any further modifications.

### 2.2.1 Synthesis of Resorcinol Formaldehyde Xerogel

Resorcinol was dissolved in formaldehyde by stirring for 15 min. Thus prepared solution was then added to an aqueous solution of potassium carbonate and continuously stirred for 15 min to prepare resorcinol formaldehyde (RF) sol. The molar ratio of resorcinol to formaldehyde, resorcinol-to-water and resorcinol-to-catalyst molar ratios were 0.25, 0.037 and 25 respectively. The graphitizing catalyst iron (II) acetate (1% w/w) was then added to as prepared RF sol and stirred for another 15 min inside glove box with an inert atmosphere. Thus prepared sol was then air dried at room temperature for 24 h followed by oven drying at 80 °C for a day to yield RF xerogel.

### 2.2.2 Pyrolysis of Resorcinol Formaldehyde Xerogel

Dried RF xerogel blocks were pyrolyzed in graphitizing tubular furnace (Materials Research Furnace, USA). After introducing the sample into the furnace tube, the tube was evacuated to 100 m Torr pressure before purging with argon gas. After purging the chamber twice, argon gas flow was maintained throughout the pyrolysis process at the rate of 2 l/min. Initially the temperature was raised to 500 °C at a ramp of 10 °C/min to prevent crack formation in RF xerogel block due to rapid mass loss. Then the furnace temperature was raised to 1800 °C with 50 °C/min ramp followed by a dwell time of 1hr at the same temperature. The samples were then cooled to room temperature in the presence of argon flow. Thus RFCX is obtained.

### 2.2.3 Ball Milling

RFCX blocks was first crushed in a mortar. Crushed samples were then filled into ball mill container with 3 mm diameter SS balls. Powder to ball weight ratio was maintained to be 1:12. The samples were milled using planetary ball mill (pulversette7, FRITSCH). The duration of milling was varied from 15 min to 12 h. The samples were labelled as RFCX-15, RFCX-45, RFCX-240 and RFCX-720 where last numeric number represents duration of milling in minutes.

### 2.2.4 Electrode Preparation

For electrochemical studies, SS foil was used as current collector. A slurry was prepared by dissolving 10% polyvinylidene fluoride (PVDF) and 90% milled carbon xerogel powder in N-Methyl -2-pyrrolidone (NMP) solvent. The working electrode was prepared by coating this slurry on SS foil followed by vacuum drying at 120 °C and lithium foil was used as a counter electrode. Glass microfiber filter (Whatman, Grade GF/D) soaked with LP-30 electrolyte was used as separator between two electrodes and packed inside the argon filled glove box using Swagelok cell assembly. Before electrochemical testing, the electrochemical cells were soaked for 12 h. Potentiostat/

Galvanostat (Bio-Logic Science Instruments, Model VSP) was used to study the electrochemical performance of packed half-cells.

## 2.3 Characterization

Field emission scanning electron microscope (FESEM, SUPRA 40 Zeiss) and high resolution transmission electron microscopy (HRTEM) (FEI Tecnai G2S-Twin) were used to study the morphological changes in RFCX structure. Powder X-ray measurements were recorded in scattering angle range of 10° to 60° on PANalytical X-ray diffractometer with CuKα radiation to study the crystallinity of the sample. Surface area of milled powders were measured in Micromeritics ASAP 2020 physisorption analyser using BET method. Pore size distribution were obtained by BJH method. The ball-milled powders were degassed at 200°C for 1 h under vacuum before performing the nitrogen absorption-desorption studies.

### 2.3.1 FESEM Characterization
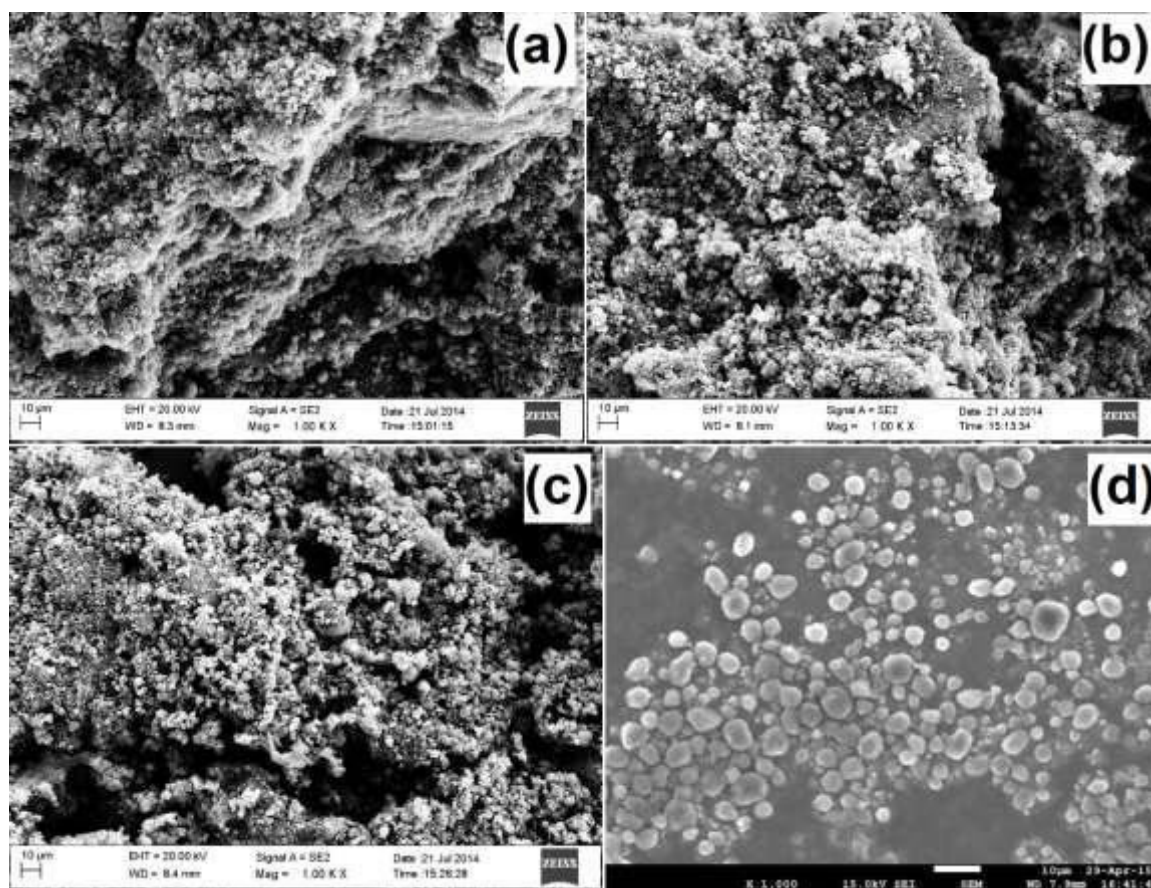


Figure 2: FESEM images of a) RFCX-15; b) RFCX-45; c) RFCX-240; and d) RFCX-720

8

Characterization by FESEM (Fig.2) for all the samples milled up to 240 mins revealed agglomeration possibly due to the reduction in particle size while milling. Although we observed that particles became finer with increased ball milling time however these were still agglomerated. As particle size decreases, the surface energy of the particles increases and overcomes the applied mechanical energy and starts agglomerating. The onset of agglomeration has been quicker when compared to graphite samples (16). This is observed because these graphitized samples has smaller crystallite size ($L_c$) and higher d-spacing (Table I) as compared to pure graphite which made RF derived carbon xerogels more prone to shear exfoliation during grinding. RFCX – 720 showed no signs of agglomeration, they were distinct particles of sizes between 2 -5 microns. As observed from Fig. 3e and Fig.3f, with increased milling we obtained graphene .These graphene layers if not separated properly will restack due to van der Waals force (26) .This restacking has increased the particle size well above the critical size required for agglomeration and thus no agglomeration was observed.

### 2.3.2 HRTEM characterization

TEM images (Fig.3) clearly reveals two kinds of regions namely graphitic region and disordered region. The graphitic region consists of well stacked larger crystallites (8-15 layers) while the disordered areas consists of randomly arranged smaller crystallites (3-6 layers) of graphene. The sample RFCX-15, consists majorly of graphitic regions and very less amount of disorder regions (Fig.3a).From the sample RFCX-45 we can observe that the stacking length is decreased indicating the broken remnants of larger stacks and an increase in disorder (Fig.3b). The RFCX-240 sample comprises mainly of disordered regions indicating the exfoliation of graphitic regions (Fig.3c). The RFCX-720 revealed graphene layers restacking and forming crystallites. Thus it can be observed that there is decrease in disorder and increase in crystallinity which can be observed in XRD as well (Table 1).
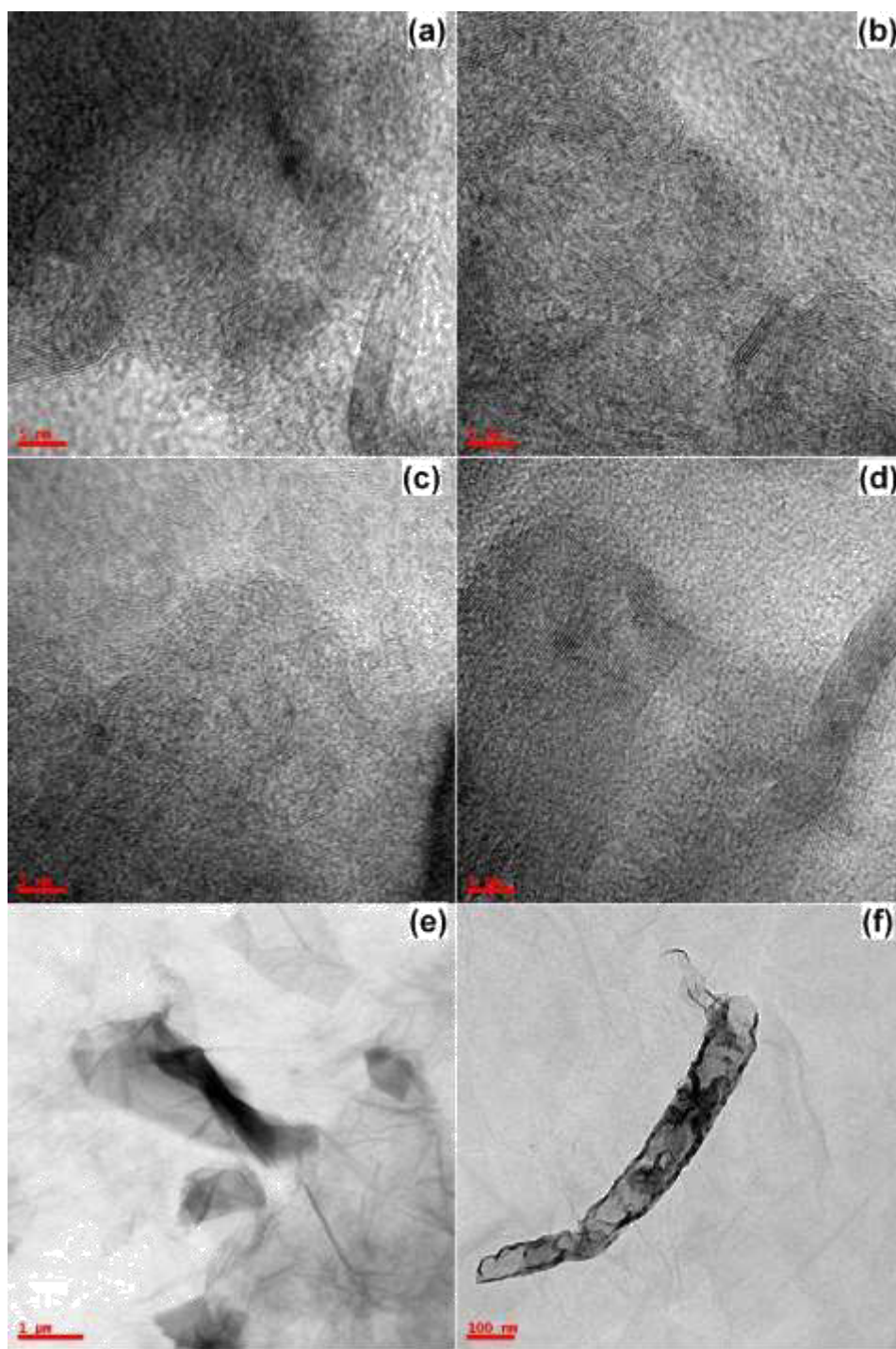
Figure 3: HRTEM images of a) RFCX-15; b) RFCX-45; c) RFCX-240; d) RFCX-720 showing restacking; e) and f) RFCX-720 showing graphene layers at different magnifications.

### 2.3.3 Characterization by XRD
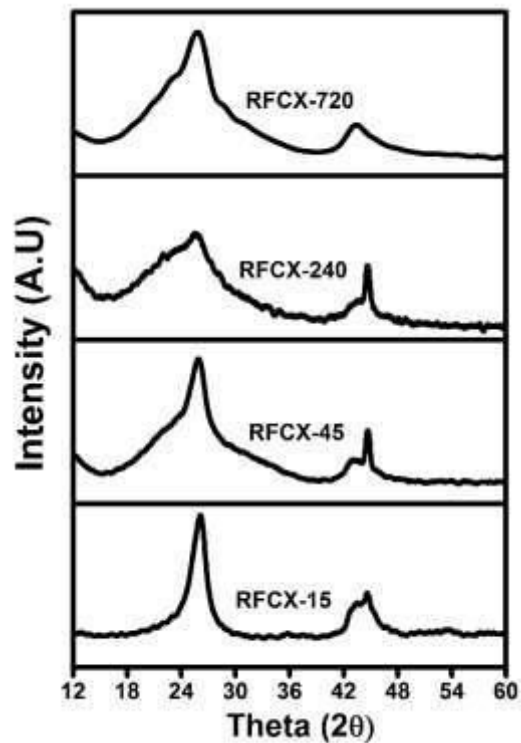


Figure 4: XRD plot of RFCX samples ball milled for different duration

Table I: Summary of XRD results of RFCX samples ball milled for different duration

| Sample | d-spacing (Å) | Peak (2θ) | Crystallite size $L_c$ (Å) | Number of Layers in stack |
|---|---|---|---|---|
| 15 | 3.38 | 26.3 | 55 | 16 |
| 45 | 3.42 | 26.0 | 27 | 8 |
| 240 | 3.45 | 25.7 | 11 | 3 |
| 720 | 3.44 | 25.9 | 16 | 5 |

Two characteristic peaks are observed in XRD plot (Fig.3). The peak near to 26° and 44° correspond to diffraction from (002) plane and (101) plane respectively (27). A well-defined sharp peak near to 26° indicates the highly crystalline nature. We can observe from Fig 4 that the sample RFCX-15 shows a sharp peak near 26° and with increase in milling time up to 240 mins the peak near 26° becomes broader. From Table I, we observe that the peak corresponding to (002) plane shifts to lower angle and d-spacing for the (002) plane increases with milling time up to 240 mins indicating the decrease in crystallinity. Also the crystallite size along the c-axis as calculated using Scherrer's formula (28) for the (002) plane and the

11

number of crystallites layers (calculated by dividing from crystallite size with d-spacing) keeps on decreasing up to 240 mins indicating shearing along the (ab) axis. From the decrease in crystallites size, we can infer that as the crystallite size decreases the duration of milling required to exfoliate the crystallite structures further also increases. This is because as the crystallite size decreases, the number of small crystallites increases and particle size also decreases and the surface energy increases and therefore more mechanical energy is required to break these crystallites further. From Table I we can observe a trend that is a decrease in crystallinity up to 240 mins but for RFCX-720 the trend reverses. The peak corresponding to (002) planes shifts to higher thetas, d-spacing decreases and crystallite size and no of stacking layers increases indicating an increase in crystallinity. This improvement in crystallinity is attributed to restacking of graphene layers.

### 2.3.4 BET Characterization

RF derived carbon xerogel possess high surface area (100-600 m$^2$/g) and porosity due to the synthesis conditions (29, 30). During graphitization at higher temperatures there is pore shrinkage and as well as decrease in surface area (31). Hard carbons have many closed pores in their structure (32, 33). The pores might have been blocked because of formation of crystallites by the rearrangement of graphene layers. From Table II, it is observed that during milling the surface area and the pore volume increases with increase in milling. This increase in surface area for RFCX-45 may be attributed to increase in the number of crystallites formed and also due to increase in pore volume. The increase in pore volume for RFCX-45 may be due to the opening of closed pores present and also due to formation of new pores due to disordered arrangement of graphite crystallites. During milling as crystallites might have broken which previously might have been blocking the pores. Thus increased milling facilitated the accessibility of such closed pores. Although there was no significant increase in pore volume after 45 min milling however surface area increased. This can be attributed to increase in number of crystallites but with reduced size. No observable change in pore volume for RFCX-240 milling indicates that the mechanical energy needed to fracture the smaller crystallites to induce pore formation is higher than the milling energy provided. Therefore more formation of pores was denied however milling ensured that all the closed pores might have been rendered accessible. The decrease in surface area for RFCX-720 is because of increase in particle size (Fig.1d) and slight increase in pore volume might be attributed to pore formation as a result of milling for 720 mins.

TABLE II: Summary of BET results of RFCX samples ball milled for different duration

| Milling time (min) | BET surface area ($m^2$/g) | BJH desorption pore volume ($cm^3$/g) |
|---|---|---|
| 15 | 112 | 0.15 |
| 45 | 273 | 0.38 |
| 240 | 348 | 0.38 |
| 720 | 262 | 0.39 |

## 2.4 Electrochemical Performance of RFCX Samples

## 2.4.1 Galvanostatic charge/discharge cycling at 0.1 C Rate

TABLE III: Summary of specific capacities of ball milled RF derived carbon xerogel samples at 0.1C rate

| Milling time (min) | First cycle | | | After 100 cycles | |
|---|---|---|---|---|---|
| | Reversible Capacity (mAh/g) | Irreversible capacity (mAh/g) | Coulombic efficiency (%) | Reversible Capacity (mAh/g) | Coulombic efficiency (%) |
| 15 | 298 | 540.7 | 35.5 | 167 | 97 |
| 45 | 386 | 422.8 | 47.7 | 158 | 98 |
| 240 | 628.8 | 614.9 | 50.6 | 242 | 98 |
| 720 | 413 | 443 | 48.3 | 180 | 99 |
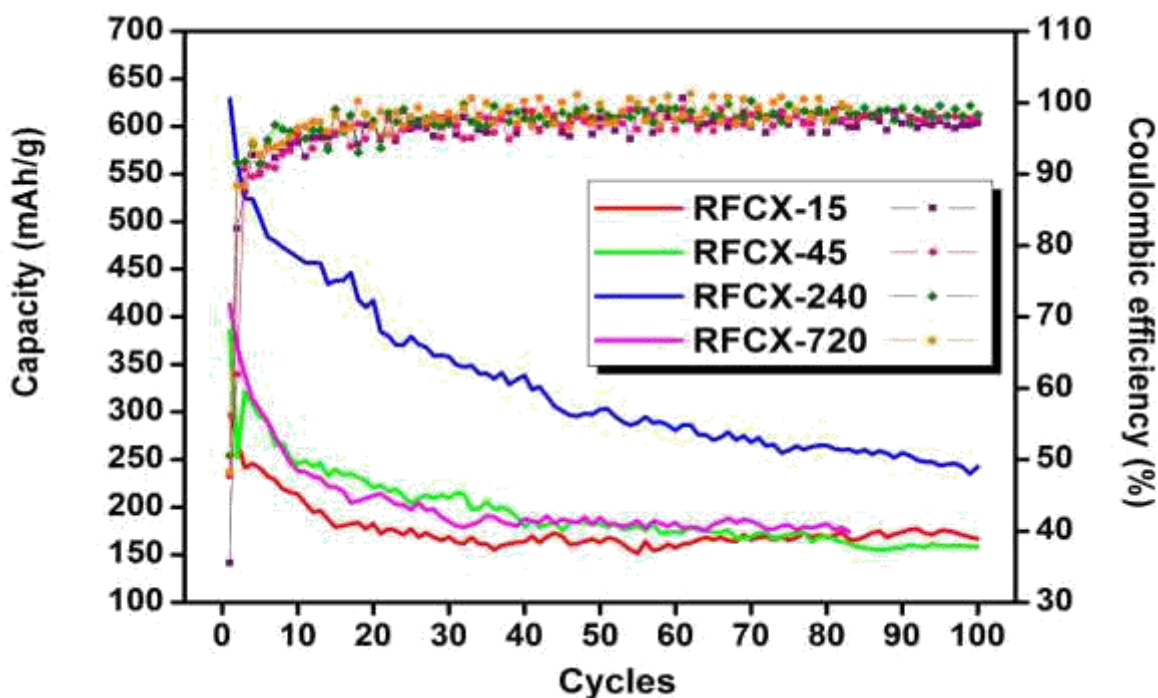
Figure 5: Comparison of cycling behavior at 0.1 C rate for RFCX ball milled for different duration

The first cycle reversible capacity (~ 630 mAh/g) and coulombic efficiency (~51%) was significantly higher for RFCX-240. Considering the significant irreversible capacity losses associated with solid-electrolyte interface formation in carbon samples in general, first cycle efficiency achieved here is quite large. Although there was more capacity fade, RFCX-240 was stabilized at 242 mAh/g reversible capacity with 98 % coulombic efficiency. This excellent electrochemical behavior of ball milled RFCX samples can be well explained with their structural characteristics.

From XRD and TEM studies, we clearly observed that the RFCX-15 sample is the most crystalline among the three. Predominately the contribution to the capacity arises due to intercalation mechanism. The first cycle irreversible loss is high mainly due to large surface area. Capacity fade in this sample could be attributed to its high porosity. If a sample is porous, the electrolyte tends to get accumulated in the pores which serves as a reaction site for the Li-ions to react and thus continuously form a passive layer (8). This passive layer impedes the Li-ions thus blocking them from accessing the insertion or intercalation sites and sometimes the Li-ions are trapped inside the pores (33) and thus causing an irreversible loss of Li-ions.

14

We earlier found RFCX-45 sample to be more porous with both graphitic and disordered regions in its microstructure. This increase in structural disorder may be linked to enhanced capacity for RFCX-45 samples as compared to RFCX-15. Further though the surface area increased, the increase in the irreversible capacity was not that significant (Table II). This may be again due to increase in disorder which might have offset the capacity loss due to increase in surface area during first cycle which is also indicated by an increase in first cycle coulombic efficiency from 35.5 to 47.7%.

The RFCX -720 sample is similar to RFCX-45 .They are also porous with a mixture of graphitic and disordered regions. The decrease in disorder and increase in crystallinity has decreased the capacity with milling after 240 mins. This is observed with a decrease in columbic efficiency from 50.6 to 48.3%.

The RFCX-240 sample exhibited higher capacity than other three samples (RFCX-15, RFCX-45 and RFCX-720). This may be because of formation of smaller crystallites which might be arranged in a very random manner like house of cards model (6). Although crystallinity was less as observed by XRD and TEM analysis however capacity is mainly due to Li ion absorption inside the pores created by random stacking of graphene layers. This hypothesis is also supported by increased surface area and large pore volume.

## 2.4.2 C-Rate capability

The Li-ion intercalation is a slow process as the Li-ions have to overcome the van der Waals force and intercalate into the lattice structure. This is the reason for reduced capacity at higher C-rates. However insertion mechanism due to disorder is different and Li-ions can insert and de insert into the host structure rapidly even at higher C-rates. This is clearly evident while testing RFCX samples ball milled for more time as shown in Fig. 6a and Fig. 6b. Even at higher C-rates (0.2, 0.5 and 1 C), RFCX-240 showed much improved capacity. At 1 C rate, reversible capacity was observed to be 200 mAh/g that is significantly higher than for RFCX-45 and RFCX-720. This value is quite significant as compared to graphitic carbon samples. Further when cycled at 0.1 C rate back, a significantly higher capacity (415 mAh/g) was retained. This excellent capacity retention (85%) is quite remarkable which can be attributed to disordered microstructure of RF derived carbon xerogel upon ball milling for sufficient time.
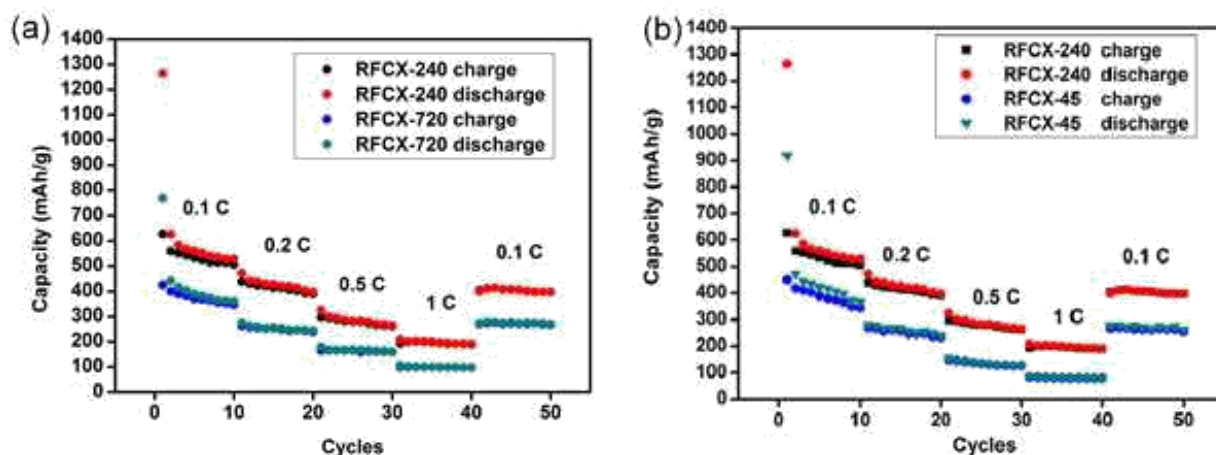
Figure 6: Comparison of C-rate capability of a) RFCX -240 and RFCX- 720; and b) RFCX-240 and RFCX-45.

### 2.4.3 Cyclic Voltammetry
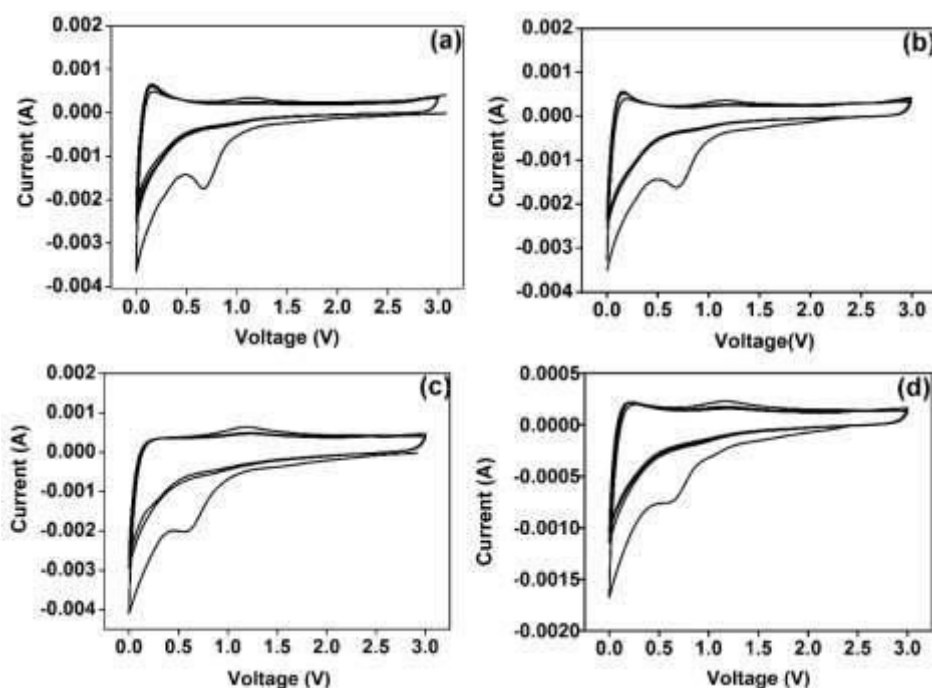


Figure 7: Cyclic voltammetry study a) RFCX – 15; b) RFCX – 45; c) RFCX- 240; and d) RFCX -720.

The cathodic current peak at 0.6 V in the first cycle indicates the SEI layer formation and the peak near 0 V corresponds to Li intercalation in all three samples. The anodic peak at 0.2 V corresponds to Li de-intercalation and the peak at 1.2 V (34) may be attributed to de-insertion from disordered microstructure. As observed in Fig. 7, the peak due to de-intercalation is

16

sharp for RFCX-15, RFCX-45 and RFCX-720 samples which was broadened for RFCX-240 sample. Similarly, the peak due to Li de-insertion due to disordered structure was well expressed in RFCX-240 sample as compared to two other samples. This observation is in line with microstructural properties of these samples as discussed above and clearly suggest that the contribution to capacity for RFCX-240 is more from disorder mechanism rather than intercalation.

## 2.5 Conclusions

Ball milling of graphitized RF derived carbon xerogel provided a tight control in tuning their microstructure and therefore crystallinity. We then studied in detail about their electrochemical performance and discussed the role of their microstructure in deciding the mechanism for Li ion reversible capacity. This study not only facilitates the efficient use of RF derived carbon xerogels as anode material for Li ion batteries by significantly improving their reversible capacity but also explore their potential use in high rate application.

# Chapter 3

# PVDF derived Carbon Powder as Anode for Lithium Ion Battery

## 3.1 Introduction

Polyvinylidene fluoride or polyvinylidene difluoride (PVDF) is a fluoropolymer comprising of monomer vinylidene difluoride. It is well known for its ferroelectric and piezoelectric property. It is a thermoplastic polymer and is semi-crystalline. PVDF exhibits polymorphism. (35) It has two chain conformations Trans (T) and Gauche (G). Depending on the linkage it may exists in different forms, some forms are alpha (TGTG'), beta (TTTT), and gamma (TTTGTTTG') phases.

PVDF has been blended with other polymers and has been used as a gel based polymer electrolytes (36) and membrane based electrolytes (36). It has also been used as a separator (37). However the most widely used application in Li-ion batteries is the role of binder. PVDF binds the active electrode material to the current collector and ensures there is no current loss due to loss of contact between the electrode and current collector.

Carbon derived from PVDF is very porous and is used for gas storage (38, 39). The process of getting carbon from PVDF involves a dehydrofluorination step. In this the fluorine is partially removed. Complete removal of the fluorine is achieved by optimizing the extent of dehydrofluorination and pyrolysis temperature (38, 40). This step also acts a thermal stabilization step as PVDF has a melting point of 190°C (41). The carbon derived from PVDF has been used as an anode for lithium ion battery. The difficulties faced were low yield of carbon and high irreversible capacity (42).

Dehydrofluorination reaction occurs is carried out in an aqueous base solution. The reaction is further accelerated by a phase transfer catalyst (43) which enhances the diffusion of the PVDF from polymer phase to aqueous phase .The significant indications for the reactions are color change from light brown to black in color. The reaction involves the transfer of

hydroxyl group to the polymer chain and removal of fluorine leading to formation of conjugated carbon bonds (44)

Our aim is to explore this PVDF as a carbon precursor and test it as anode for Li-Ion battery applications. We have studied the effect of atmosphere on dehydrofluorination. We also evaluated the changes in functional groups and crystallinity during carbonization and correlated its effect with electrochemical performance.

## 3.2 Materials and methods

*Materials*

Sodium Hydroxide (97% purity), LP-30 electrolyte (1 M $LiPF_6$ in 1:1 v/v mixture of ethylene carbonate and diethyl carbonate) were procured from Merck, India. Lithium foil (99.9% trace metal basis) and Poly (vinylidene fluoride) (PVDF) (99.9% purity), was procured from Sigma Aldrich, India. Tetra-n-butyl ammonium bromide (TBAB) (98% purity) was procured from Alfa Aesar, India. We used stainless steel (SS) foil (polycrystalline SS 316, 100 µm thick) as current collector and procured the same from MTI corp., USA. Deionized water was used as solvent for preparing sodium hydroxide solution. All chemicals were used directly without any further modifications.

### 3.2.1 Dehydrofluorination

1 gm. of PVDF powder was added to 40 ml solution containing 4M NaOH and 12.5mM TBAB under inert atmosphere inside a glove box or in the presence of atmosphere. The solution was kept under constant stirring for 2 hours at 70° C. The solution turns black in color which indicates the onset of reaction. After the reaction, the aqueous phase is removed from polymer phase by filtration followed by successful washing with ethanol and methanol. The polymer phase was then oven dried at 70° C until constant weight. The samples which were dehydrofluorinated in an inert atmosphere and air were labelled as PDI and PDA respectively

### 3.2.2 Pyrolysis of dehydrofluorinated PVDF

The dehydrofluorinated powder were pyrolyzed in tubular furnace (Nabertherm, Germany). After introducing the sample into the furnace tube, the tube was purged with nitrogen gas. After purging the chamber twice, nitrogen gas flow was maintained throughout the pyrolysis process at the rate of 2 l/min. The temperature was ramped from room temperature to desired

temperature at 5°C/min and then dwelled at the same temperature for 1 hour. The samples were then cooled to room temperature in the presence of nitrogen. Carbons obtained by pyrolysis of PDI and PDA were labelled as CDI-X and CDA-X. The X is used to denote the pyrolysis temperature. The samples were labelled as CDI-900, CDI-1200 and CDA-900

### 3.2.3 Electrode Preparation

For electrochemical studies, SS foil was used as current collector. A slurry was prepared by dissolving 10% polyvinylidene fluoride (PVDF) and 90% CDI-X in N-Methyl -2- pyrrolidone (NMP) solvent. The working electrode was prepared by coating this slurry on SS foil followed by vacuum drying at 120 °C and lithium foil was used as a counter electrode. Glass microfiber filter (Whatman, Grade GF/D) soaked with LP-30 electrolyte was used as separator between two electrodes and packed inside the argon filled glove box using swagelok cell assembly. Before electrochemical testing, the electrochemical cells were soaked for 12 h. Potentiostat/ Galvanostat (Bio-Logic Science Instruments, Model VSP) was used to study the electrochemical performance of packed half-cells.

### 3.3 Characterization

Raman spectrum was recorded with a 532 nm laser using Bruker Raman microscope spectrometer to study the crystallinity of sample (Model: Senterra). Fourier Transform Infrared spectroscopy (FTIR, Bruker Tensor 37) was recorded in the range 600-4000 cm-1 range with a resolution of 4 cm−1 to observe the changes in functional groups.

### 3.3.1 FTIR Characterization

To understand the effect of atmosphere on dehydrofluorination reaction. We performed the reaction in presence of air and inert atmosphere. FTIR characterization provided us information about the changes in the chemical structure after the reaction. The pure PVDF (Fig. 8a) comprises of α and ß isomers. Dehydrofluorination was performed with NaOH as the base and TBAB as the phase transfer catalyst because the catalytic activity was found to be more efficient. (43). The indicators for dehydrofluorination reaction to take place are formation of conjugated double bonds between carbon, decrease in intensity of characteristic peaks from $1400 cm^{-1}$ to $500 cm^{-1}$(43) and formation of hydroxyl functional groups (44). Although, fluorine peaks found at $1112 cm^{-1}$ in PVDF disappeared and the intensity of the peaks between $1400 cm^{-1}$ to $600 cm^{-1}$ diminished in both cases (Fig. 8b and Fig. 8c).

The hydroxyl group found in the region between 3700 cm$^{-1}$ -3200 cm$^{-1}$ and the aromatic (C=C) bond found between 1600cm$^{-1}$ and 1400cm$^{-1}$ were more intense in the case of PDI (Fig. 8b) than PDA (Fig. 8c). This suggests that inert atmosphere to be the best for performing the dehydrofluorination reaction.
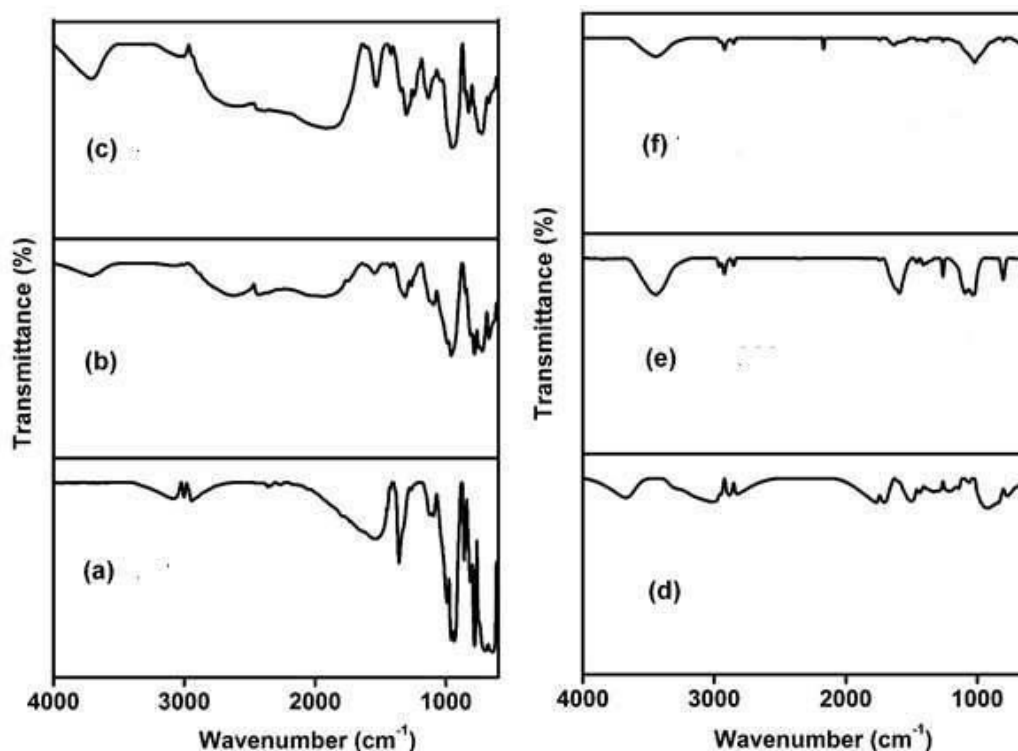


Figure 8: Comparison of FTIR spectrum of a) PVDF; b) PDA; c) PDI; d) CDA-900; e) CDI-900; and f) CDI-1200

To compare the effect of carbonization on both PDA and PDI, they were pyrolyzed at the same temperature at 900°C. All peaks corresponding to fluorine were removed in case of CDI-900 but one peak at 768cm$^{-1}$ was found in CDA-900. This peak was found in case of PDA as well. But the other peak that was found near 615cm$^{-1}$ in case of both PDA and PDI was not found in both the pyrolyzed samples. And also the peak corresponding to the aromatic bond formation was more intense in CDI than CDA. This confirms that sample dehydrofluorinated in inert atmosphere is the best for carbonization. If we compare the CDI-900 and CDI-1200, we can observe that hydroxyl OH functional groups (3700 cm$^{-1}$-3200 cm$^{-1}$) and C-O functional groups (1300 cm$^{-1}$ -1000cm$^{-1}$) were decreasing and carbonyl C=O (1820 cm$^{-1}$-1670 cm$^{-1}$) were forming with increasing temperature. C-C triple bond ( 2260 cm$^{-1}$-2100cm-1) was also found for CDI-1200.

21

## 3.3.2 RAMAN Characterization
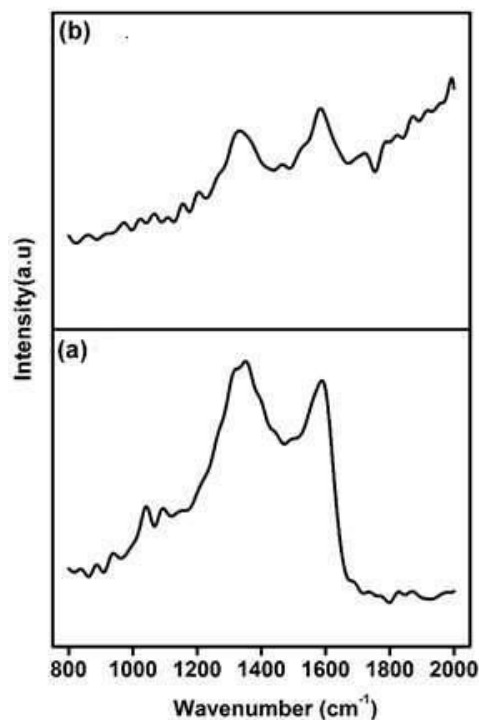


Figure 9: Comparison of RAMAN spectrum of   a) CDI-900; and b) CDI-1200

TABLE IV: Summary of RAMAN results of CDI samples pyrolyzed at different temperatures.

| Sample | $I_d/I_g$ | $L_a$ |
|---|---|---|
| CDI-900 | 1.1 | 4.1 |
| CDI-1200 | 0.9 | 4.9 |

The Raman spectrum is used to probe the sp2 hybridized structure and quantitate the amount of the disorder by calculating the ratio of intensity of D band and G band .The D band arises due to the disorder in the structure and appears near $1350 cm^{-1}$ .The D band corresponds to A1g breathing mode .The G band appears at about $1583 cm^{-1}$ and corresponds to E2g mode. The Id/Ig ratio decreased and La increased (Table IV) with increase in temperature (Fig.9). This indicates that increase in temperature has increased the crystallinity of the sample. This is because higher temperature induces graphitization of the sample. This also suggests that the carbon derived from PVDF is a hard carbon

22

## 3.4 Electrochemical performance of CDI samples

### 3.4.1 Galvanostatic Charge/discharge Cycling at 0.1 C Rate

TABLE V: Summary of specific capacities of CDI samples pyrolyzed at different temperatures at 0.1 C- rate

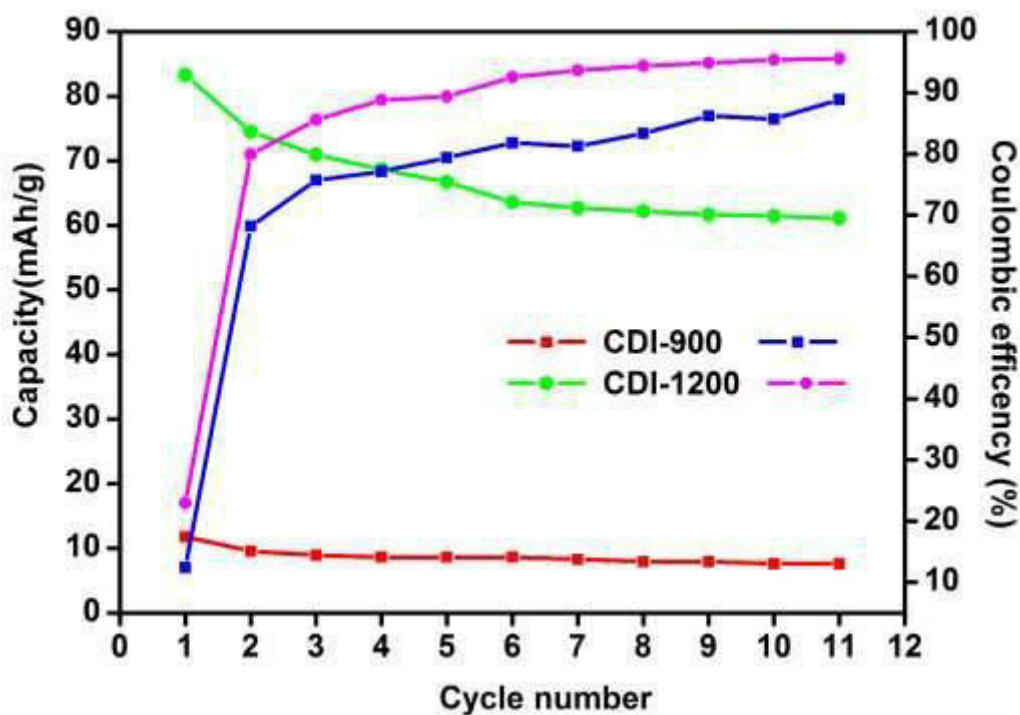| Sample | First cycle | | | After 11 cycles | |
|---|---|---|---|---|---|
| | Reversible Capacity (mAh/g) | Irreversible capacity (mAh/g) | Coulombic efficiency (%) | Reversible Capacity (mAh/g) | Coulombic efficiency (%) |
| CDI-900 | 12 | 83 | 12.4 | 8 | 89 |
| CDI-1200 | 83 | 279 | 23 | 61 | 96 |



Figure 10: Comparison of cycling behavior at 0.1 C rate for CDI samples pyrolyzed at different temperatures

CDI- 900 showed very poor capacity. This is attributed due to the amorphous nature as indicated by RAMAN (Table IV).The first cycle irreversible capacity is high.(Table V). This

23

is due to SEI layer formation due to electrolyte decomposition at low voltages. The initial columbic efficency is also poor.

CDI-1200 performed better than the CDI-900 sample. This is because of improvement in crystallinity (Table IV) which has resulted an increase in intercalation capacity which is observed in CV as well (Fig.11b). The high irreversible capacity in both the samples is attributed to oxygen containing functional groups.(10,45) The carbonyl groups are present in addition to the other functional groups in CDI-1200 which has caused a further increase in irreversible capacity (10,45).Though there was an improvement in capacity with increase in temperature. The capacity is still insignificant.

### 3.4.2 Cyclic Voltammetry

In CDI-900 there are two cathodic current peaks corresponding to SEI layer (Fig.11a) at 1.1 V and 1.5 V. While in CDI-1200 the peaks due to SEI are found at 0.35V and 0.7 V (Fig.11b). The peak near 0 V corresponds to Li-ion intercalation .The anodic peak at 0.2 V is sharper in CDI-1200 than CDI-900. This peaks corresponds to intercalation and this is well expressed because of improved crystallinity of sample. (Table IV). The anodic peak at 1.2 V corresponds to de-insertion of Li-ions from disordered structures. This peak is well expressed in CDI 900 indicating that the capacity is due to absorption of Li-ions on the surface.
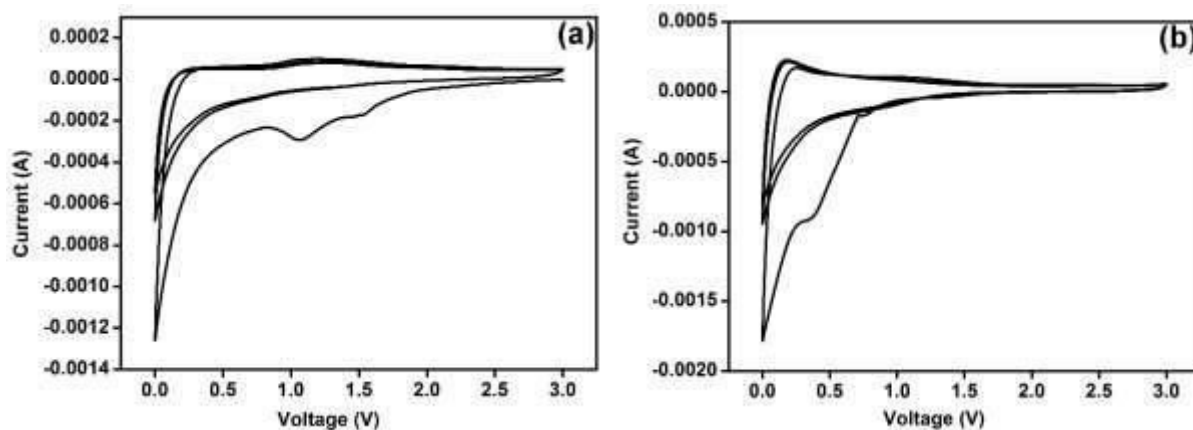


Figure 11: Comparison of Cyclic Voltammetry of  a) CDI-900 and b) CDI-1200

### 3.5 Conclusions

The carbon yield from PVDF has significantly improved to 70% due to dehydrofluorination step which had acted as a thermal stabilization step. From the structural analysis we can conclude that the carbon obtained is a hard carbon. With pyrolysis the hydroxyl and the ester

24

functional groups decrease but carboxyl functional groups are increased. The change in crystallinity has improved the capacity but the higher irreversible capacity is attributed to the carboxyl groups. Though the capacity has increased it still remains insignificant .But the material has responded well to heat treatment which suggest that further graphitization will enhance the capacity.

# Chapter-4

# Summary and Future Directions

## 4.1 Summary

In this thesis, we have mainly discussed how the hard carbon microstructure can be tailored to enhance its capacity as anode. The unique aspect is that we have dealt with two opposite process one reducing the crystallinity (milling) and the other enhancing the crystallinity (graphitization). We have seen how the interplay of crystallinity, morphology, surface functional groups, particle size, porosity, surface area contribute to the electrochemical performance. A brief review of various carbon materials is also elucidated in chapter 1.In the preceding chapter we have explained in detail the synthesis, characterization and electrochemistry of the aforementioned hard carbons

### 4.1.1 Fine tuning of hard carbon microstructure

In the second chapter we have ball milled hard carbon (RFCX) for different duration .We milled to an extent until complete exfoliation is achieved .In the third chapter we first partially dehydrofluorinated the carbon precursor (PVDF) and then pyrolyzed at different temperatures. By dehyrdrofluorinating we were able to improve the yield of carbon. Thus we were able to tailor the structure by these two synthesis methods.

### 4.1.2 Characterization

The hard carbon microstructure and chemical composition was studied by various characterization. In chapter 2, with the help of FESEM we were able to observe whether the samples were agglomerated or not .This was important for us to understand the particle size changes with milling. HRTEM characterization provided information about the graphitic and disordered regions. It also supported XRD results by visually showing the crystallite size changes. Further it confirmed the presence of crumpled graphene layers and its restacking. XRD results helped us to understand the changes in crystalline structure .It provide valuable information regarding the average spacing between two layers, crystallite size, no of layers in

the stack. The BET surface area measurement was useful to correlate the changes in surface area with changes in particle size and BJH pore volume changes confirmed that milling improves the accessibility of closed pores. In chapter 3, Raman characterization quantitatively showed the changes in disorder and confirm the improvement in crystallinity. FTIR provided us information about the functional groups changes during dehydrofluorination and carbonization by which we were able to determine that inert atmosphere is the best condition for dehydrofluorination. It also showed the presence of carboxyl groups had a detrimental effect on capacity.

### 4.1.3 Electrochemical performance

In chapter 2, The ball milled sample with the most disorder showed higher capacity This is due to House of cards model .We were able to confirm this phenomena by cyclic voltammetry as well. Ball milling not only improved the capacity but also improved the rate capability. The samples further showed a high recovery capacity when reverted back to low C-rate. This suggests structure to be stable and suitable for High C-rate applications .Ball milling provided us a control tool to tailor the desired microstructure for optimum performance. In chapter 3, though the capacity of PVDF derived hard carbon was insignificant it showed improvement with increasing temperature .This is attributed to the increase in crystallinity. Thus we were able to demonstrate the potential of PVDF derived carbon as anode for Li-ion battery.

### 4.2 Future Directions

i) The main challenge impeding the usage of hard carbons is the capacity fade observed which was even observed in the ball milled samples as well as graphitized samples. If we could address the issue by doing some chemical treatment or by synthesizing composites, it would be vital in further enhancing the hard carbon usage for both high and low C rate applications.

ii) Graphene is obtained by graphite by wet ball milling or in the presence of shear exfoliants. We were able to obtain graphene in 12 hrs by dry ball milling without any addition of exfoliants .This is significant when compared to graphite which takes much longer time .To the best of our knowledge there was no previous reports on obtaining graphene from resorcinol formaldehyde carbon xerogel. Thus a further study in this direction would enable us to obtain graphene from a new source which could make it cheaper.

iii) We demonstrated that carbon obtained after dehyrdrofluorinating PVDF could be used as anode for Li-ion battery .By carefully optimizing the extent of dehydrofluorination and graphitization conditions we can modify the surface functional groups and improve its capacity. Graphitization can be achieved by pyrolysis at high temperatures or by means of a catalyst.

iv) PVDF can be electrospun and cast as a film as well. So by nanostructuring, we can further change the morphology and improve its electrochemical performance further.

# References

[1] T. P. Kumar, T. S. D. Kumari, and A. M. Stephan. Carbonaceous anode materials for lithium-ion batteries - the road ahead. J Indian Inst Sci 89, (2009) 393–424.

[2] M. B. Pinson and M. Z. Bazant. Theory of SEI formation in rechargeable Batteries : capacity fade, accelerated aging and lifetime Prediction. J Electrochem.Soc 160, (2013) A243–A250.

[3] D. S. Su and R. Schlogl. Nanostructured carbon and carbon nanocomposites for electrochemical energy storage applications. ChemSusChem 3, (2010) 136–168.

[4] J-M. Tarascon and G. G. Amatucci. Microengineering aerospace systems. 1st edition. The Aerospace Press, 1999.

[5] Z. Ogumi and M. Inaba. Advances in lithium ion batteries. 1st edition. Kluwer Academic Publishers, 2002.

[6] Y. Liu, J. S. Xue, T. Zheng, and J. R. Dahn. Mechanism of lithium insertion in hard carbons prepared by pyrolysis of epoxy resins. Carbon 34, (1996.) 193–200.

[7] M. Kakunuri, S. Vennamalla, and C. S. Sharma. Synthesis of carbon xerogel nanoparticles by inverse emulsion polymerization of resorcinol formaldehyde and their use as anode materials for lithium-ion battery. RSC Adv 5, (2015) 4747–4753.

[8] V. Agubra and J. Fergus. Lithium ion battery anode aging mechanisms. Materials 6, (2013) 1310–1325.

[9] Y. P. Wu, E. Rahm, and R. Holze. Effects of heteroatoms on electrochemical performance of electrode materials for lithium ion batteries. Electrochim. Acta 47, (2002) 3491–3507.

[10] W. Lu and D. D. L. Chung. Effect of the pitch-based carbon anode on the capacity loss of lithium-ion secondary battery. Carbon 41, (2003) 945–950.

[11] R.Janot and D. Guerard. Ball-milling in liquid media applications to the preparation of anodic materials for lithium-ion batteries. Prog. Mater. Sci 50, (2005) 1–92.

[12] F.Disma, J. Tarascon, C. Clinard, and J. Rouzaud. Transmission electron microscopy studies on carbon materials prepared by mechanical milling. Carbon 37, (1999) 1941–1959.

[13]  X. H. Chen, H. S. Yang, G. T. Wu, M. Wang, F. M. Deng, X. B. Zhang, J. C. Peng, and W. Z. Li. Generation of curved or closed-shell carbon nanostructures by ball-milling of graphite. J. Cryst. Growth 218, (2000) 57–61.

[14]  T. Fukunaga, K. Nagano, U. Mizutani, H.Wakayama, and Y.Fukushima. Structural change of graphite subjected to mechanical milling. J.Non. Cryst. Solids 232–234, (1998) 416–420.

[15]  Y. Chen, J. F. Gerald, L. T. Chadderton, and L. Chaffron. Nanoporous carbon produced by ball milling. Appl. Phys. Lett 74, (1999) 2782-2784.

[16]  F. Disma, L. Aymard, L. Dupont, and J.-M.Tarascon. Effect of mechanical grinding on the lithium intercalation process in graphites and soft carbons. J. Electrochem. Soc 143, (1996) 3959-3971.

[17]  V.Leon, A.M. Rodriguez, P. Prieto, M. Prato, and E. Vazquez Exfoliation of graphite with triazine derivatives under ball-milling conditions : Preparation of few-layer graphene via selective noncovalent interactions. ACS Nano 8, (2014) 563–571.

[18]  F.S.Disma, C.Lenain, B. Beaudoin, L. Aymard, and J.M-Tarascon. Unique effect of mechanical milling on the lithium intercalation properties of different carbons. Solid State Ionics 98, (1997) 145–158.

[19]  R. Alcantara, P. Lavela, G. F. Ortiz, J.L.Tirado,, R. Menendez, R. Santamarıa, and M. Jimenez-Mateos. Electrochemical, textural and microstructural effects of mechanical grinding on graphitized petroleum coke for lithium and sodium batteries. Carbon 41, (2003) 3003–3013.

[20]  C. S. Wang, G. T. Wu, and W. Z. Li. Lithium insertion in ball-milled graphite. J. Power Sources 76, (1998) 1–10.

[21]  W. Xing, R. A. Dunlap, and J. R. Dahn. Studies of lithium Insertion in ball milled sugar carbons. J. Electrochem. Soc 145, (1998) 62–69.

[22]  C. Natarajan, H. Fujimoto, A. Mabuchi, K. Tokumitsu, and T. Kasuh. Effect of mechanical milling of graphite powder on lithium intercalation properties. J. Power Sources 92, (2001) 187–192.

[23]  S. A. Al-muhtaseb and J. A. Ritter. Preparation and properties of resorcinol-formaldehyde organic and carbon gels. Adv. Mater 15, (2003) 101–114.

[24] X. Yuan, Y-J. Chao, Z. Ma, and X.Deng. Preparation and characterization of carbon xerogel (CX ) and CX − SiO composite as anode material for lithium-ion battery. Electrochem. Commun 9, (2007) 2591–2595.

[25] C. S. Sharma, H. Katepalli, A. Sharma, G. T. Teixidor, and M. J. Madou. Fabrication of resorcinol-formaldehyde xerogel based high aspect ratio 3-D hierarchical C-MEMS structures. ECS Trans.61, (2014) 45–54.

[26] R. Aparna, N. Sivakumar, A. Balakrishnan, A. S. Nair, S. V Nair and K. R. V Subramanian. An effective route to produce few-layer graphene using combinatorial ball milling and strong aqueous exfoliants. J. Appl. Phys 5, (2014) 033123-1 -033123-11.

[27] T. S. Ong and H. Yang. Effect of atmosphere on the mechanical milling of natural graphite. Carbon 38, (2000) 2077–2085.

[28] B. Manoj and A. G. Kunjomana. Study of stacking structure of amorphous carbon by X-ray diffraction technique. Int. J. Electrochem. Sci 7, (2012) 3127-3134.

[29] E. A. Oyedoh, A. B. Albadarin, G. M. Walker, M.Mirzaeian and M. N. M. Ahmad. Preparation of controlled porosity resorcinol formaldehyde xerogels for adsorption applications. Chem. Eng. Trans 32, (2013) 1651–1656.

[30] C. Lin and J. A. Ritter. Effect of synthesis pH on the structure of carbon xerogels. Carbon 35, (1997) 1271–1278.

[31] F.J.Maldonado- Hodar, C.Moreno-Castilla, J.Riveria-.Utrilla, Y. Hanzawa and Y. Yamada. Catalytic graphitization of carbon aerogels by transition metals. Langmuir 16, (2000) 4367–4373.

[32] K. Gotoh, M. Maeda, A. Nagai, A. Goto, M. Tansho, K. Hashi, T. Shimizu, and H. Ishida. Properties of a novel hard-carbon optimized to large size Li ion secondary battery studied by Li NMR .J. Power Sources 162, (2006) 1322–1328.

[33] K.Guerin, M.Menetrier A.Fevrier-Bouvier, S. Flandrois, B. Simon, and P. Biensan. A ^{7}Li NMR study of a hard carbon for lithium − ion rechargeable batteries. Solid State Ionics 127, (2000) 187–198.

[34] H. Kataoka, Y. Saito, O. Omae, J. Suzuki, K.Sekine,T.Kawamura and T.Takamura. Lithium storage mechanism of disordered mesophase carbon fibers Studied by [7]Li-Nuclear Magnetic Resonance. Electrochem. Solid-State Lett 5, (2002) 10–13.

[35]  W.A.Yee, M. Kotaki, Y. Liu, and X. Lu. Morphology, polymorphism behavior and molecular orientation of electrospun poly (vinylidene fluoride ) fibers. Polymer 48, (2007) 512–521.

[36]  S.W. Choi, S.M. Jo, W.S. Lee and Y-R. Kim. An Electrospun Poly(vinylidene fluoride) nanofibrous membrane and its battery applications. Adv. Mater 15,(2003) 2027–2032.

[37]  S-S. Choi, Y.S.Lee, C.W.Joo, S.G.Lee, J. K.Park, and K-S. Han. Electrospun PVDF nanofiber web as polymer electrolyte or separator. Electrochim. Acta 50, (2004) 339–343.

[38]  S-M. Hong, S. H. Kim, B.G. Jeong, S.M..Jo and K.B.Lee. Development of porous carbon nano fibers from electrospun polyvinylidene fluoride for $CO_2$ capture. RSC Adv 4, (2014) 58956–58963.

[39]  S.E.Hong, D-K. Kim, S.M.Jo, D. Y.Kim, B. D.Chin, and D.W.Lee.Graphite nanofibers prepared from catalytic graphitization of electrospun poly ( vinylidene fluoride ) nanofibers and their hydrogen storage capacity. Catal. Today 120, (2007) 413–419.

[40]  Y. Yang, A. Centrone, L. Chen, F. Simeon, T. A. Hatton, and G. C. Rutledge. Highly porous electrospun polyvinylidene fluoride (PVDF) based carbon fiber. Carbon 49, (2011) 3395–3403.

[41]  J. Yamashital, M. Shioya, T. Kikutani, and T. Hashimoto. Activated carbon fibers and films prepared from poly (vinylidene fluoride) by using a chemical carbonization. Carbon 39, (2001) 207–214.

[42]  T. Zheng, Y. Liu, E. W. Fuller, S. Tseng, U. Von Sacken, and J. R. Dahn. Lithium insertion in high capacity carbonaceous materials. J. Electrochem. Soc 142, (1995) 2581–2590.

[43]  H.Kiese and H.Ogata. Phase transfer catalysis in dehydrofluorination of poly(vinylidene fluoride) by aqueous sodium hydroxide solutions. J. Polym. Sci., Part A: Polym. Chem. 21, (1983) 3443-3451.

[44]  J. Wootthikanokkhan and P. Changsuwan. Dehydrofluorination of PVDF and proton conductivity of the modified PVDF / sulfonated SEBS blend membranes. J. Metals, Mater. Miner.18, (2008) 57–62.

[45]   C. Fu, G. Zhao, H. Zhang, and S. Li. Evaluation and characterization of reduced graphene oxide nanosheets as anode materials for lithium-ion batteries. Int. J. Electrochem. Sci. 8, (2013) 6269–6280.